Nanoscale

PAPER

Cite this: *Nanoscale*, 2015, **7**, 1491

Determination of a refractive index and an extinction coefficient of standard production of CVD-graphene†

Efraín Ochoa-Martínez,*[a] Mercedes Gabás,[a] Laura Barrutia,[b] Amaia Pesquera,[c] Alba Centeno,[c] Santiago Palanco,[a] Amaia Zurutuza[c] and Carlos Algora[b]

Received 16th October 2014,
Accepted 26th November 2014

DOI: 10.1039/c4nr06119e

www.rsc.org/nanoscale

The refractive index and extinction coefficient of chemical vapour deposition grown graphene are determined by ellipsometry analysis. Graphene films were grown on copper substrates and transferred as both monolayers and bilayers onto SiO_2/Si substrates by using standard manufacturing procedures. The chemical nature and thickness of residual debris formed after the transfer process were elucidated using photoelectron spectroscopy. The real layered structure so deduced has been used instead of the nominal one as the input in the ellipsometry analysis of monolayer and bilayer graphene, transferred onto both native and thermal silicon oxide. The effect of these contamination layers on the optical properties of the stacked structure is noticeable both in the visible and the ultraviolet spectral regions, thus masking the graphene optical response. Finally, the use of heat treatment under a nitrogen atmosphere of the graphene-based stacked structures, as a method to reduce the water content of the sample, and its effect on the optical response of both graphene and the residual debris layer are presented. The Lorentz–Drude model proposed for the optical response of graphene fits fairly well the experimental ellipsometric data for all the analysed graphene-based stacked structures.

Introduction

The study of the unique properties of graphene has been the main goal of many studies during the last few years. Its great potential in a large number of applications[1] and moreover, as a transparent conductor in a variety of optoelectronic devices (such as LEDs, solar cells, touch screens, *etc.*)[2,3] makes graphene a likely substitute for indium tin oxide (ITO) or any other transparent conductive oxide (TCO).[4] The most promising method for obtaining large scale layers of graphene with high quality optoelectronic properties is by chemical vapour deposition (CVD).[5]

Graphene optical properties have been the goal of an extensive list of studies in the last few years. Optical spectroscopies in the range of the infrared[6] and visible/ultraviolet[7] spectrum are regular tools used in the characterisation of graphene optical properties. Optical transmission and reflection have also been extensively used.[8,9]

The optical behaviour of twisted bilayer graphene has been studied by Raman spectroscopy[10] and optical conductivity measurements.[11] Recently, graphene optical properties have found an application in photonic materials,[12] and differential transmission spectra have been used to explore the electron–acoustic phonon coupling.[13]

It is thus crucial for the inclusion of graphene at an industrial optoelectronic level that its transparency and optical behaviour are well understood. From the bibliography, it is possible to infer that the optical behaviour of graphene differs significantly depending on the production technique, whether it has been exfoliated[14–16] or deposited through chemical vapour deposition;[17–19] furthermore, that the diverse substrates used like metals,[17] semiconductors[14] and insulators,[9,14,16,20,21] may they be transparent[18] or opaque, put in an additional variable to make a proper comparison of graphene's optical behaviour. Finally, for the case of transferred graphene, a layer of transferred residues seems to form between the substrate and graphene[18] which affects the optical response and should be deducted in order to obtain the results for pristine graphene. Therefore, the optical performance of deposited graphene cannot be determined without taking into account the substrate, the growing method, residual impurities and the transfer process. The consideration of real graphene optical properties is a key issue when designing graphene-based optoelectronic devices. Alternatively, methods for the removal of

[a]*Universidad de Málaga, The Nanotech Unit, Departamento de Física Aplicada I, Campus de Teatinos, 29071 Málaga, Spain. E-mail: e8am@uma.es*
[b]*Instituto de Energía Solar, Universidad Politécnica de Madrid, Avda. Complutense 30, 28040 Madrid, Spain*
[c]*Graphenea S.A., Tolosa Hiribidea 76, 20018 Donostia-San Sebastián, Spain*
†Electronic supplementary information (ESI) available: DETAILS. See DOI: 10.1039/c4nr06119e

contaminants that contribute to the quality of graphene are of paramount importance.

In this work, the optical response of graphene grown by CVD and afterwards transferred onto SiO_2/Si substrates has been analysed using a combination of Angle Resolved X-ray Photoelectron Spectroscopy (ARXPS) and Spectroscopic Ellipsometry (SE). The purpose of the ARXPS analysis is to determine the real stacked structure after graphene is transferred to the desired substrate. The aim is to analyse the optical response of commercially available graphene, which has been grown in a large scale facility, taking into account the effects of: (a) the interactions between graphene and the substrate, (b) stacking more than one monolayer of graphene, (c) the residues from the transfer process that could degrade the properties of graphene and the accuracy of the measurements, and (d) the thermal treatment. The final objective of this work is to obtain the optical properties of large scale produced graphene, transferred to other substrates using a standard procedure, with a high enough accuracy, and the determination of the contribution of residual layers to the graphene optical characteristics.

The following section accounts for the technical characteristics of the experimental equipments and technologies used for the fabrication and characterisation of the studied samples, where a special emphasis will be made on the graphene transfer process. The third section presents the experimental data and discusses the main results obtained after the analysis. The ARXPS analysis subsection helps to find the real stacked structures obtained after a standard transfer process of the graphene layers. In the Optical properties subsection, we present first of all a deduction of the graphene optical characteristics by considering an ideal structure after the transfer process of a graphene layer onto a SiO_2/Si substrate. We show how the refractive index (n) and extinction coefficient (k) values vary depending on several parameters of the stacked structure. After this, we present the extracted graphene optical parameters using as input the real stacked structures, deduced after the ARXPS analysis of a monolayer and a bilayer graphene. To conclude, we show how a thermal process could help to eliminate the contamination layers formed during the transfer process and how the experimental data are influenced.

Experimental

The analysed samples have been grown on copper (Cu) foils by CVD and transferred onto SiO_2/Si wafers.[22] Graphene synthesis was carried out in a cold walled CVD reactor (Aixtron BM) at 1000 °C and at low pressure using methane as the carbon source. Prior to the growth the Cu foils were annealed at 1000 °C under hydrogen and argon flow. After the synthesis, a poly(methyl methacrylate) (PMMA) support layer was spin coated onto the graphene covered Cu foil. Cu was etched using a ferric chloride containing solution and the monolayer graphene was transferred onto the final substrate. Finally, the PMMA layer was removed by dipping into acetone. The synthesized graphene films were characterized using Transmission Electron Microscopy (TEM), Raman spectroscopy and optical microscopy. This is a very well established method to assess the quality of graphene. In Fig. 1(top), a TEM image shows the hexagonal lattice structure of monolayer graphene along with some typical features of CVD grown graphene such as grain boundaries. In order to obtain these images, the monolayer graphene was transferred onto Quantifoil TEM Grids. The image was taken in high resolution TEM mode at 80 kV using a Titan G2 60-300 with an image Cs-corrector. On the other hand, the Raman spectrum in Fig. 1(bottom) shows the typical fingerprint of monolayer graphene. The spectrum was recorded using a WiTec Confocal Raman Microscope with a 532 nm laser wavelength. In order to carry out the Raman characterization the graphene film was transferred onto a 300 nm SiO_2/Si substrate. More information about the as-grown graphene can be found in the ESI.† Some of the samples were transferred onto a thin native oxide that in this paper will be referred to as MLG (monolayer graphene), while others were transferred onto a thick thermal oxide, referred to as MLG-TO. The bilayer graphene (BLG) sample was produced by repeating the monolayer transfer process twice. Fig. 2 shows the nominal stacked structures expected after the transfer process.

In order to determine the deviation of the real stacked structures from the nominal ones shown in Fig. 2, a surface

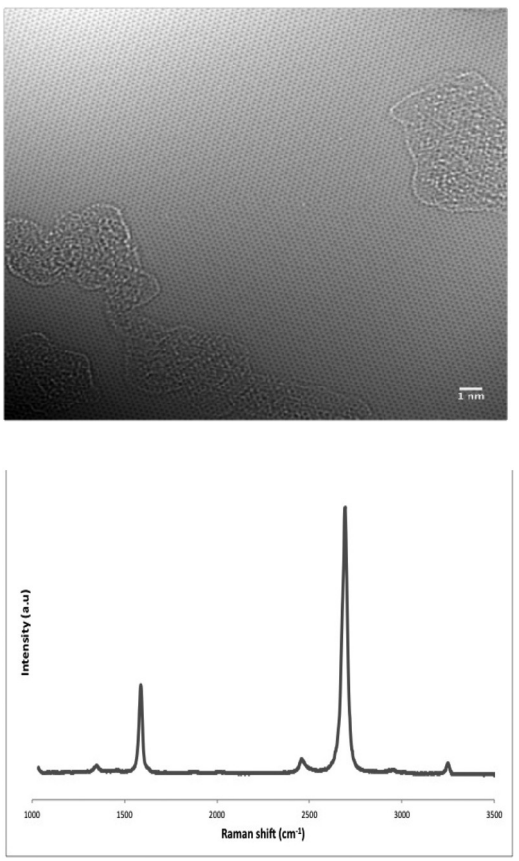

Fig. 1 High resolution TEM images of CVD monolayer graphene (top). Raman spectrum corresponding to monolayer graphene (bottom).

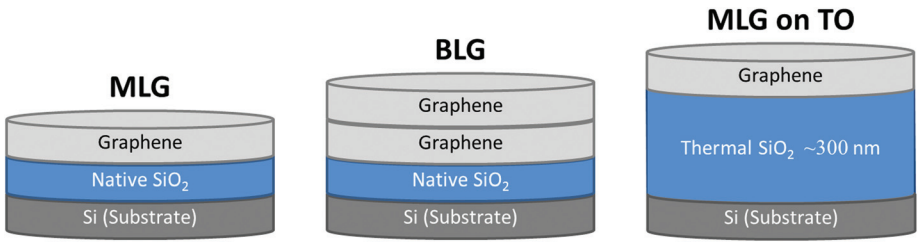

Fig. 2 Nominal layered structures for monolayer and bilayer samples (not to scale).

analysis by ARXPS was carried out using a Thermo Scientific Multilab 2000 spectrometer, fitted with a dual anode (Mg-Kα, Al-Kα) X-ray source and a 110 mm mean radius hemispherical sector analyser. No Ar^+ sputtering was made to clean up sample surfaces, which were measured as received in order to not disrupt the sp^2 network.[23] In order to explore the evolution of the surface composition on top of, and under the graphene layer, measurements were made at three different take-off angles (10°, 45° and 90°, outside the photoelectron pathway measured from the sample surface), thus changing the explored depth. The core level spectra were fitted using the XPSPeak software package.[24]

The optical properties have been analyzed through Variable Angle Spectroscopic Ellipsometry (VASE) in a Semilab GES-5E ellipsometer in the region from 210 to 980 nm, the spot size of the ellipsometer varies between 1 and 4 mm depending on the signal to noise ratio and the incident angle, which varies between 60° and 75°. Measurements of the polarization state (ψ, Δ) have been made at room temperature on the samples as-received. Additionally, MLG samples have been measured after each step of the thermal process consisting of one hour annealing under a nitrogen atmosphere, first at 150 °C, and then in order to evaluate the reversibility of the process, two weeks later at 250 °C. The adjustment and fittings have been carried out using the Spectroscopic Ellipsometric Analyser (SEA) software v.1.3.0, and the optical parameters of the rest of the materials present in the structure (silicon, silicon oxide and water) have been obtained from the database included in the software.[25] All the measurements and analysis have been repeated on several equivalent samples obtaining fully comparable results.

Results and discussion

ARXPS analysis

Firstly, the analysis of the as-grown graphene on copper foils (see ESI†) for a 10° take-off angle (*i.e.* the explored depth is always less than 1 nm) revealed a clean surface with no traces of either oxygen or any other contaminants on top of graphene. However, as the explored depth increased a small signal from O–C bonds appeared both in the C 1s and O 1s core level signals (see ESI†). Both facts strongly suggest that the top surface of the as-grown graphene layer is free from contaminants, which would be a proof of its quality, but there is some oxygen trapped under the graphene layer.

The transferred graphene layers onto native SiO_2/Si substrates (MLG sample) show the presence of transfer debris on top of the graphene surface. At the C 1s core level, the C–O signal in the data taken at 10° doubles its intensity, *i.e.* more than 20% of the peak signal, when compared to the data taken at 45° and 90°, *i.e.* around 10% of the total peak signal (see

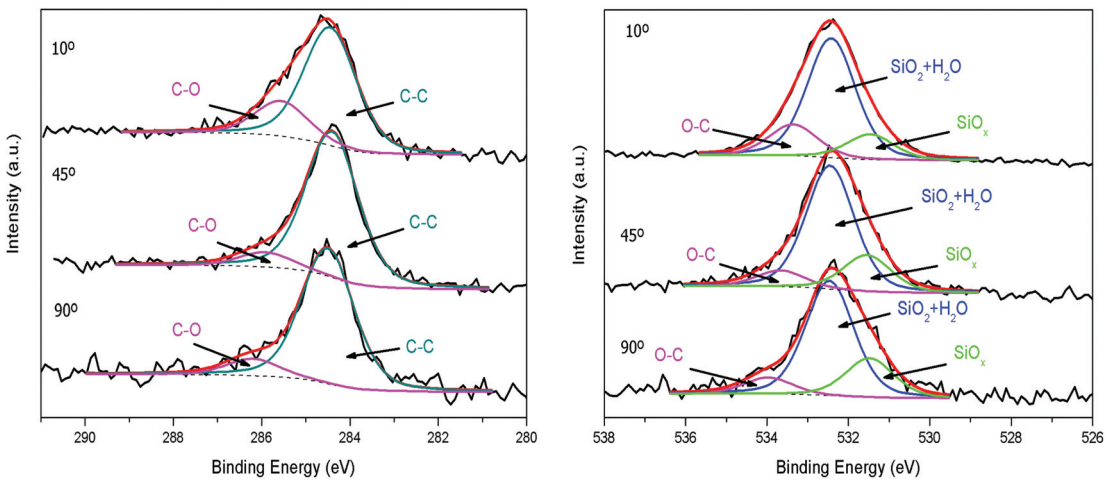

Fig. 3 Deconvolution of C 1s (left) and O 1s (right) core level signals in their constituents, for the MLG sample. Take-off angle, and therefore explored depth, increases from top to bottom.

Fig. 3, left). This is a proof of the presence of carbons linked to the oxygen on top of the graphene surface. Thus, after the transfer process, graphene layers seem to be sandwiched between two contamination layers. It should be taken into account that CVD graphene layers on Cu are not perfectly flat[26] and this fact would favour the appearance of these residual layers. The evolution of the O 1s core level signal with the explored depth indicates that adsorbed water is an important constituent of these residues. Oxygen anions in SiO_2 and H_2O share the same binding energy region, and their contributions are indistinguishable, that is the reason why the central contribution to the O 1s core level signal does not change its intensity with the explored depth. SiO_2 contribution should increase in intensity as the explored depth increases; therefore, H_2O contribution should follow the opposite behaviour. For this sample, the data taken at 45° and 90° are almost equal, leading to very similar deconvolutions. This fact, together with the analysis of the Si 2p signal (see ESI†) allows the estimation of the distance from the sample surface to the non-oxidised Si substrate, to be a bit smaller than 3 nm. That would include the transfer residues on top of the graphene surface, the graphene monolayer itself and the contamination layer trapped under the graphene layer.

Samples of monolayer graphene transferred onto Si/thermal SiO_2 (MLG-TO) show the presence of C–O, C═O and O–C═O bonds suggesting the PMMA polymer debris on top of the graphene layer and they contribute both to C 1s and O 1s core level signals (see ESI†). About 15% of the C 1s signals at the lowest take-off angle are due to this precursor debris. Their intensity strongly diminishes with the explored depth, which indicates that its presence is restricted to the contamination layer on top of graphene. In this structure no estimation about the distance from the sample surface to the non-oxidized Si substrate can be made because of the large SiO_2 thickness (around 300 nm).

In the bilayer graphene (BLG) sample, PMMA debris is again clearly identified among the constituents of the C 1s core level signals, as is evident in Fig. 4, where contributions from C–O, C═O and O–C═O bonds can be distinguished.[27] For this sample, they can be easily detected at 45° and 90° take-off angles, and the C–O signal increases in intensity with the explored depth, which is indicative of their presence in an intermediate contamination layer between the two graphene sheets. In this case, the analysis of the Si 2p signal (see ESI†) allows an estimation of the distance from the sample surface to the non-oxidized Si substrate to be in the order of 5 nm.

Therefore, the ARXPS analysis suggests the need to include additional layers beneath and on top of the transferred graphene layers in order to better describe the real stacked structures. Accordingly, the final structures for monolayer and bilayer samples evolve from those of Fig. 2 to those of Fig. 5. The structure for MLG and MLG-TO samples differs just in the SiO_2 thickness. A more detailed description of these stacked structures will be given in the following subsection.

Optical properties

The general procedure for making ellipsometric data analyses begins with a proposed layered structure where the thicknesses and optical behaviours of each layer can be treated as known parameters or as the final result of the fitting procedure. In this paper, the graphene layers have been modeled with a

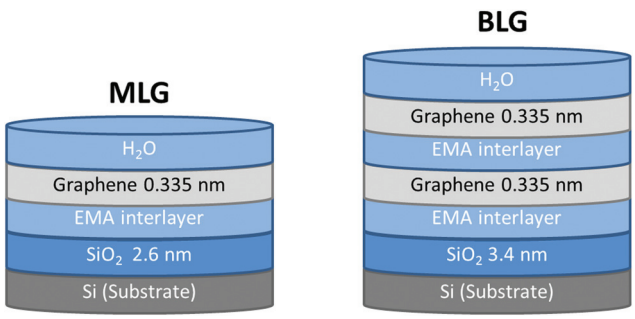

Fig. 5 Layered structures for monolayer and bilayer samples.

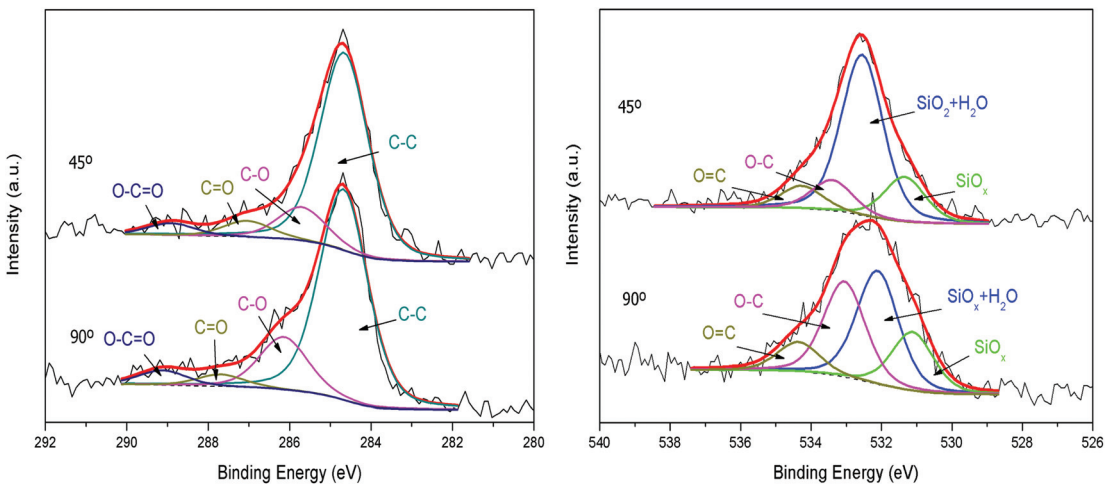

Fig. 4 Deconvolution of C 1s (left) and O 1s (right) core level signals in their constituents, for the BLG sample. Take-off angle and therefore explored depth, increases from top to bottom.

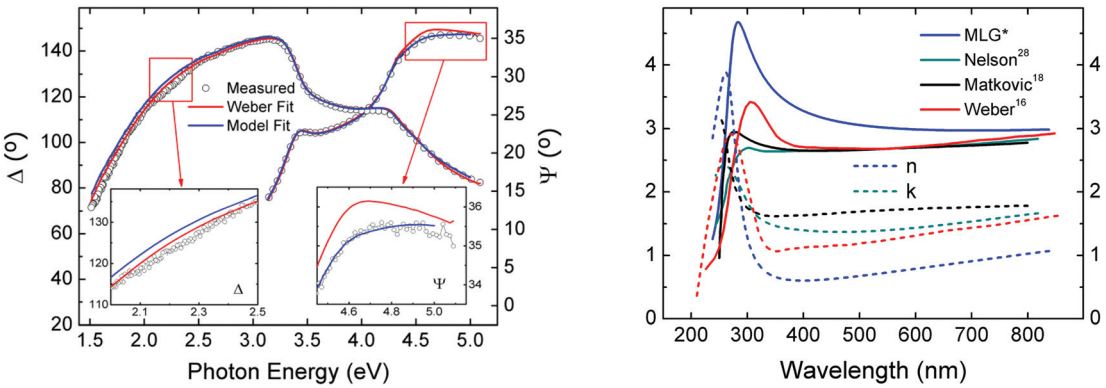

Fig. 6 Ellipsometric measurements at 75° incident angle for MLG sample deposited on oxidized silicon substrates and model fittings (left). The refractive index and extinction coefficient when considering the nominal (MLG*) structure of Fig. 2 compared with bibliographic results (right).

Lorentz oscillator for the van Hove singularity.[28] The behaviour in the near-infrared (NIR) region is represented by the Drude model[29] which can be used to describe the electrical conduction of quasi free electrons in metals or carriers in semiconductor materials. This model leaves five general terms which should be adjusted as shown in eqn (1) and (2), where ε represents the complex dielectric permittivity; E_P and E_Γ belong to the Drude part of the model and are respectively the plasma energy and the broadening, while the Lorentz peak parameters are the oscillator strength f, position E_0 and width Γ.[25] Given that neither of the terms are Kramers–Kronig consistent, the relationship between the refractive index and the extinction coefficient is purely phenomenological rather than analytical. For the sake of clarity, a detailed analysis of the MLG sample will be presented, while similar results for both BLG and MLG-TO samples can be seen in the ESI.†

$$\varepsilon_{\mathrm{Drude}}(E) = \frac{\left(\frac{E_P}{E}\right)^2}{1+\left(\frac{E_\Gamma}{E}\right)^2}\left[-1+\mathrm{i}\frac{E_\Gamma}{E}\right] \quad (1)$$

$$\varepsilon_{\mathrm{Lorentz}}(E) = \frac{f{E_0}^2}{({E_0}^2-E^2)^2+\Gamma^2E^2}\left[({E_0}^2-E^2)+\mathrm{i}\Gamma E\right] \quad (2)$$

MLG sample. Let us first illustrate the importance of taking into account the inclusion of the contamination layers. The MLG sample transferred onto native oxide has been measured on a variable angle range of 60°–75°. The uncertainty regarding the native oxide layer thickness has been limited by measuring the native oxide region not covered by the graphene layer, resulting in an oxide thickness of 2.6 nm, as is shown in Fig. 5(left). Considering the nominal structure proposed in Fig. 2, a reasonable fit for the experimental data could be achieved (Fig. 6, left). Similar results were obtained with data acquired at 60°, 65° and 70°. The two regions highlighted in Fig. 6(left) are the regions around 4.7 eV in the ψ spectrum (inset right), which is an especially sensitive region due to the van Hove singularity.[8] As an example, in the image can be seen the misfit arising from the use of the model proposed by Weber *et al.*[16] for exfoliated graphene. On the other hand, there is a misfit region at around 2.3 eV in the Δ spectrum, related to the presence of oxide and water in the sample. In spite of the fit quality, the n and k values extracted from the fitting process differ considerably from those reported in previous studies (Fig. 6, right), especially in the van Hove singularity region (200–300 nm).

Up to this point the graphene thickness has been considered a constant value (0.335 nm) and thus left out of the interpolating fitting procedure. However, considering the spot size of the ellipsometer, which varies between 1 and 4 mm depending on the incident angle and the signal to noise ratio, the probability to measure a distribution of monolayers and bilayer regions, must be taken into account. In such cases and keeping the same layered structure shown in Fig. 2, it is possible to model the effect of an increase in the average graphene thickness (Fig. 7 and ESI†). Comparing these results with the others previously reported,[16,18,28] it is evident that although a better agreement can be achieved in the near UV region, it fails in the visible range. Therefore, a variable graphene thickness would not be the reason for the inappropriate n, k values obtained after data analyses using the sample structure proposed in Fig. 2.

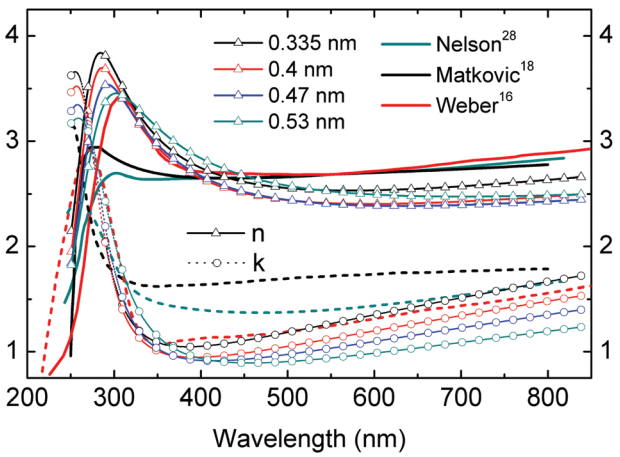

Fig. 7 Effect of graphene thickness in the model fit of n and k for graphene in the MLG sample. Some previous results are shown for comparison purposes (solid, n, and dashed, k, lines).

It is thus evident that the structure used as the input for the SE analysis should take into account the contamination layers detected in the ARXPS measurements as presented in Fig. 5. On top of the graphene surface, a contamination layer whose main constituent is water has been considered. The general trend is to consider graphene as a homogeneous and completely flat layer where the thickness is a constant value, and thus, exclude it from the interpolating fitting procedure. However, considering the relatively large spot size of our ellipsometer compared to the sample size (of the order of 1 cm^2) and the manual graphene transfer process, the probability of having a non-perfect monolayer of graphene, with irregularities in the form of very small humps,[18] must be taken into account (see Fig. 1 and ESI†). In our case a component of approximately 5% of graphene (see ESI†) has been included in the interlayers between the graphene and SiO_2 layers, representing the possible non-uniformities that could be present on the graphene surface. Then, the optical properties of these interlayers are the result of an effective medium approximation (EMA) whose main constituent is water, which could have been adsorbed during the transfer process, and graphene; the adjusted thickness of this layer is 1.1 nm. The structure is completed with a top layer of water of approximately 0.5 nm. The inclusion of such layers improves the fitting results (Fig. 8, top and middle) and modifies the optical response of the graphene layer (Fig. 8 bottom). Other materials essayed without satisfactory results as possible constituents in the interlayers have been air, carbon and PMMA; although their inclusion does not improve the SE fitting, this technique cannot completely discard their presence at very low concentrations.

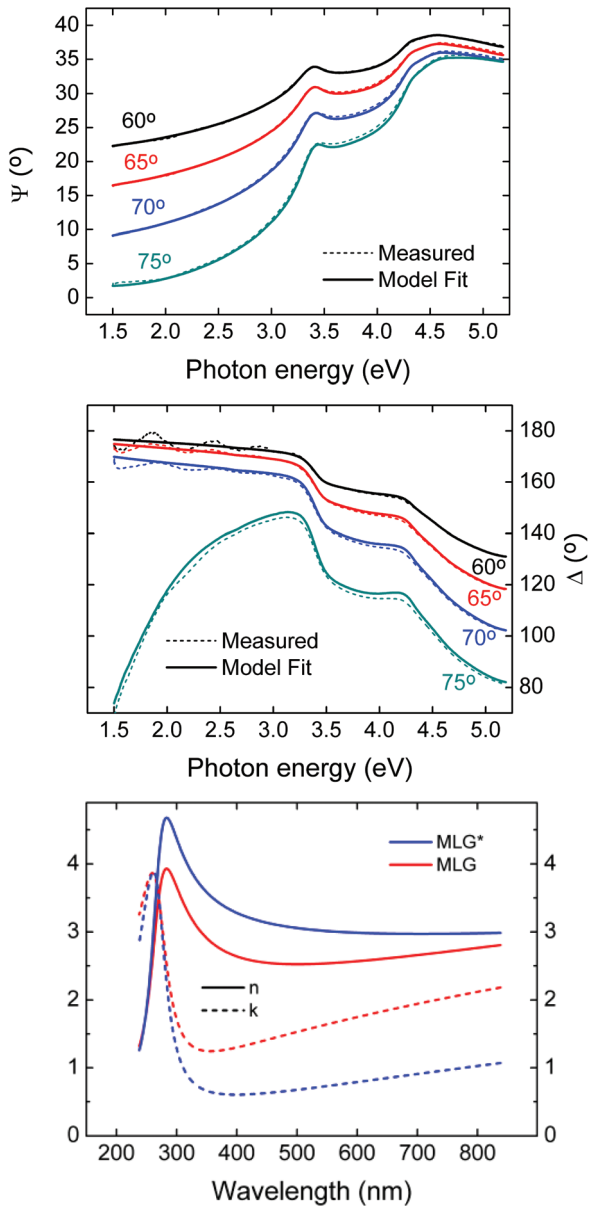

Fig. 8 VASE results, ψ (top) and Δ (middle), for the MLG sample measured from 60° to 75° incidence angle and fitting by using the layered structure of Fig. 5. Bottom, the refractive index and the extinction coefficient when considering the stacked structure of Fig. 5 (MLG) compared with those corresponding to the nominal structures in Fig. 2 (MLG*).

BLG and MLG-TO samples. The optimised model of the MLG sample has been used for the BLG structure, shown in the right hand side of Fig. 5, composed of a silicon substrate, a native oxide layer and a double stack of the water–graphene EMA interlayer and graphene. The fitting process provided a slightly thicker silicon oxide layer (3.4 nm) and a thicker water top layer (0.6 nm) when compared to the MLG sample, which agrees well with the XPS analysis. The fitting process has been improved by feedback, using the BLG results as seed data on the MLG structure adjustments. Finally, the multilayered structure and the model have been tested on the MLG-TO sample with satisfactory results.

Measured and fitted Δ acquired at 75° incident angle for all the samples are shown in Fig. 9(left), where the data for the native SiO_2/Si substrate have also been included as a reference. The image shows the good fittings produced by the model in all the cases. Furthermore, it allows comparing the effect of the graphene layers on the optical response of the Si oxide layers. The low effect of graphene on the optical response arises from its reduced thickness, so the use of a graphene double layer sample helps to overcome this issue by increasing the relative effect of graphene in the ellipsometric measurements.

Fig. 9(left) displays the high sensibility of SE by showing the effect of a monolayer and a bilayer of graphene on the Si/SiO_2. Therefore, the analysis of a single wavelength in the 2–3 eV region of Δ would allow SE to complement or substitute other techniques currently used for graphene quality control, such as AFM or Raman spectroscopy.[30] Regarding the MLG-TO sample, a major fitting disagreement arises due to a major uncertainty related to the thick oxide layer properties and a lower relative weight of graphene in comparison with such a thick oxide layer.

The refractive index and extinction coefficient of graphene deduced for each case are shown in Fig. 9(right), and the corresponding model parameters are listed in Table 1, along with the coefficient of determination (R^2) which arises from the comparison of measured and simulated data for each case (as shown in Fig. 8 for MLG). The model produces acceptable

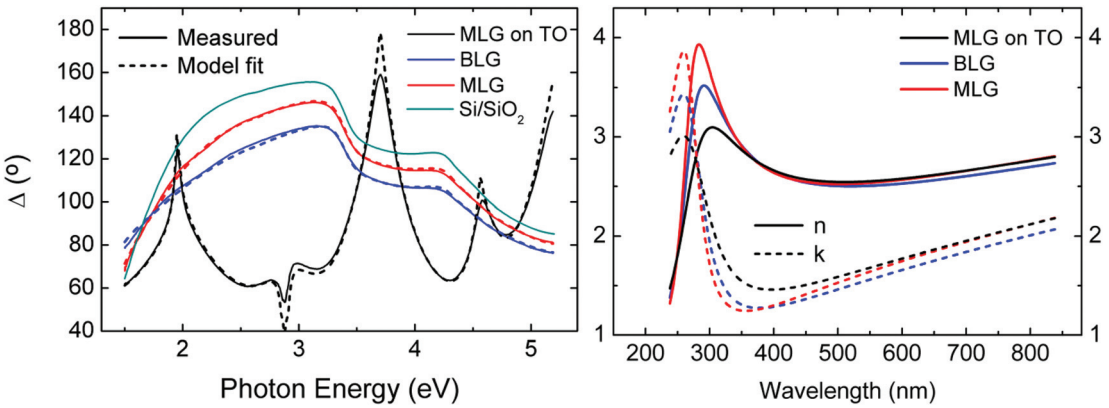

Fig. 9 Ellipsometric measurements at 75° incident angle for graphene samples deposited on oxidised silicon substrates (left). Refractive index (solid lines) and extinction coefficient (dashed lines) obtained from the models of the monolayer and bilayer samples (right).

Table 1 Parameters of the SE model used to describe the optical properties of the different graphene samples

Parameter	MLG	BLG	MLG-TO
E_p (eV)	23.14	21.13	20.48
E_{Γ} (eV)	29.99	27.33	23.97
f	3.317	3.413	3.432
E_0 (eV)	4.596	4.555	4.501
Γ (eV)	0.736	0.966	1.34
R^2	0.9984	0.9994	0.9905

agreement of n and k for the graphene present on the three structures (MLG, BLG and MLG-TO) in the visible and NIR regions of the spectrum, which are now comparable to the values obtained in these regions by some other authors.[14,16,18,19] However, in the vicinity of the van Hove singularity there is a more intense refraction and extinction for MLG than for BLG. These results are not surprising, since these differences have already been reported for single layer and bilayer exfoliated graphene. Differences in model parameters obtained after fitting could be explained by taking into account that the excitonic response at the van Hove singularity depends on the competition between e–e and e–h interactions, thus the differences on the substrate characteristics would produce variations in the position and symmetry of the UV extinction peak.[31,32] There is a decrease in the intensity of refraction and extinction once the structure of the double layer sample has been taken into account, a behaviour which is further enhanced for the MLG-TO sample, contributing to the theory that graphene–substrate, graphene–graphene or in general the interactions of graphene with the surrounding layers affect the electronic and excitonic response, which is then manifested in the macroscopic optical behaviour.

Other factors such as crystallinity, layer thickness and doping (intentional or not) might as well influence the optical response of graphene, varying the intensity of the excitonic effects and consequently the absorption profile.[33] The position and height of the extinction coefficient peak due to the van Hove singularity of some previous studies are listed in Table 2.[15] In spite of the value dispersion, there are trends that can be deduced, for example that thicker graphene layers produce a blue shift on the absorption peak, or that CVD samples result in less intense peaks than exfoliated samples, which would be a consequence of crystallinity.

When comparing our results with those that have been published, the position of the maximum in the extinction coefficient is similar to values obtained by most authors. Regarding the height, our results are in close agreement with those found in studies where the existence of transfer residues has been taken into account. However, as it has already been mentioned in this manuscript, the position, height and symmetry of the UV extinction peak is closely related to the character-

Table 2 Position and height of the main peak in the extinction coefficient according to references

Description	Thickness	Growing method	Substrate	Interlayer	eV	k	Reference
Kravets	0.335 nm	Exfoliated	Si/SiO_2	Water/air	4.79	2.74	14
Losurdo A	0.3 nm	CVD	Si/SiO_2/Ni	—	4.68	2.45	17
Losurdo F	2 nm	CVD	Si/SiO_2/Ni	—	5.15	1.94	17
Matkovic (2013)	Single layer	CVD/transferred	Sapphire	Transfer residue	4.8	3.14	18
Matkovic (2012)	Single layer	Exfoliated	Si/SiO_2	Water	4.55	2.85	15
Nelson (2010)	0.335 nm	CVD/transferred	Si/SiO_2	—	4.8	2.42	28
Nelson (2012)	4 layers	Epitaxial	SiC	SiC	4.81	2.46	19
Weber	0.34 nm	Exfoliated	Si/SiO_2	—	4.6	2.94	16
MLG	0.335 nm	CVD/transferred	Si/SiO_2	Water–graphene	4.77	3.86	This work
BLG	0.335 nm	CVD/transferred	Si/SiO_2	Water–graphene	4.78	3.42	This work
MLG-TO	0.335 nm	CVD/transferred	Si/SiO_2	Water–graphene	4.78	3.01	This work

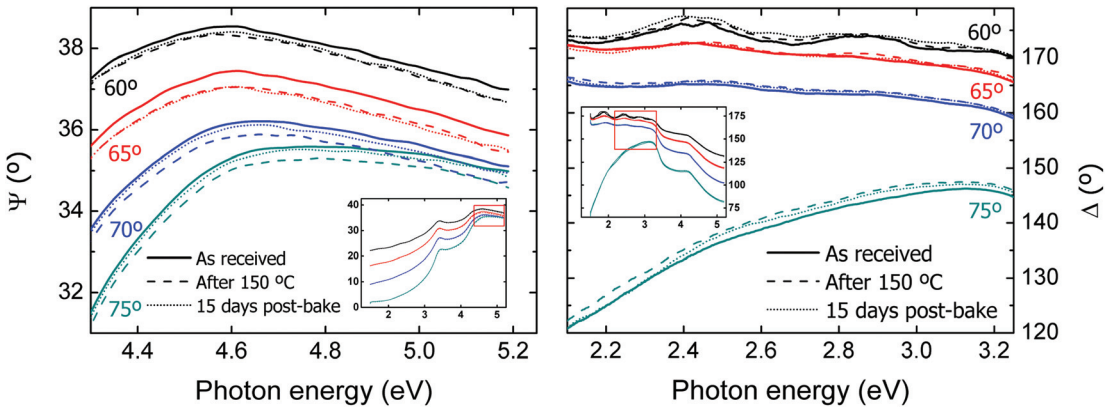

Fig. 10 VASE measurements for the MLG structure measured before and after thermal processing at 150 °C. Both figures are magnifications of the red rectangles at the insets.

istics of the substrate.[31,32] Finally, it must be taken into account that most of the optoelectronic devices (solar cells, LEDs, touch screens, *etc.*) able to incorporate graphene, operate at wavelengths higher than 300 nm where disagreements shown in Fig. 9(right) are considerably reduced.

Effect of thermal processing. After the analysis presented in the previous section, it is proved that the contamination layers associated with the transfer process of the as-grown graphene layers to any other substrate modify the optical response of the stacked structure. In some cases, it could be desirable to remove, as much as possible, these residues, in order to not deteriorate the device optical performance. For such a purpose, the simplest solution is to anneal the structures at adequate temperatures under a controlled atmosphere.

The effect of thermal processing on the optical response has been analysed, the hypothesis regarding this is that it is possible to diminish the uncertainty in the structure by reducing the residue content after the transfer process. Additionally, thermal processing would increase the quality of the layered structure by improving the transparency and the adhesion between graphene and the substrate.[18] Two thermal processes have been carried out on the MLG structure, the first one at 150 °C and the second one at 250 °C, both for one hour under a nitrogen atmosphere with a ramp up rate of 5 °C min^{-1}. As shown in Fig. 10, thermal annealing is effective even at relatively low temperatures (150 °C). The main effect can be seen on higher energies of ψ, which is an especially sensitive region due to the van Hove singularity, and in the region between 2 and 3 eV of Δ, which as mentioned before strongly evidences the presence of oxide and water in the sample. These two regions have already been highlighted in Fig. 6(left), where the misfit arising from the use of the Weber model (exfoliated graphene) with a structure lacking intermediate layers, is shown.

It is possible to measure the effect of the thermal treatment on the water content of the sample, this has been accomplished fitting the results of the VASE acquisitions at each step of the thermal treatment keeping fixed the same layered structure of the MLG shown in Fig. 5, and letting the EMA interlayer thickness as the only free variable. This procedure results in a decrease from the original 1.2 nm to 0.63 nm, approximately half the original value, after 1 hour of thermal treatment at 150 °C. After the thermal treatment, the sample absorbs humidity from the atmosphere and consequently this thickness slowly increases, consequently, five days later it is 0.65 nm and two weeks later it is 0.72 nm. It is worth mentioning here that thermal processing would probably diminish both, the EMA interlayer thickness and the thickness of the top water layer, though for the sake of simplicity, only the reduction of the first one has been considered in the data fitting.

An additional annealing at 250 °C shows a further decrease in the water content, and the residue interlayer thickness finally reaches 0.25 nm. The complete evolution can be seen in Fig. 11, where for the sake of simplicity just the results acquired at 75° of incidence angle are shown, though the behaviour is similar for all the angles. As is evident in this figure, the thickness reduction of the transfer residue layer is easily detected through the SE measurements, which could be used as a telltale sign of thermal annealing effectiveness. The progression in Fig. 10 and 11 demonstrates the close resemblance of the acquisitions five and fifteen days after the first bake with the original measurement of the sample as received, showing that the process of moisture adsorption in graphene, though steady is relatively slow and not fully reversible.

Finally, the effectiveness of thermal treatments is demonstrated in Fig. 12. The ellipsometric data obtained after the 250 °C annealing have been fitted using the nominal structure shown on the left side of Fig. 2 (*i.e.* supposing there are no contamination residues on top and under the graphene layer). The obtained refractive index and extinction coefficient (black lines in Fig. 12) are now closer to the values obtained for the data measured without thermal treatment but fitted using the real structure shown in Fig. 5 (red lines in Fig. 12). For comparison purposes, the values of the refractive index and the extinction coefficient obtained for the data measured before thermal annealing and fitted using the structures shown in Fig. 2 (blue lines in Fig. 12) are also shown. Therefore, although this thermal treatment partially removes the contamination, a consideration of the real structure (such as that

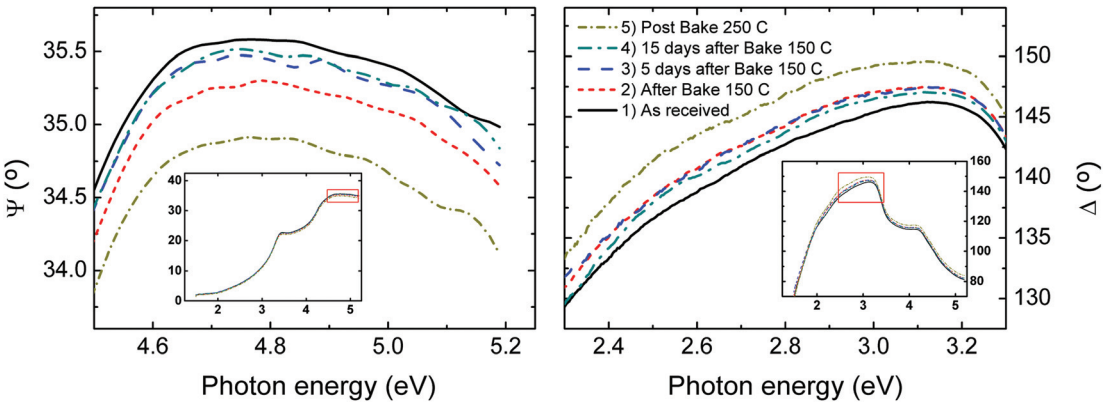

Fig. 11 Spectral ellipsometric measurements at 75° of incidence for MLG measured in the different stages of the thermal annealings.

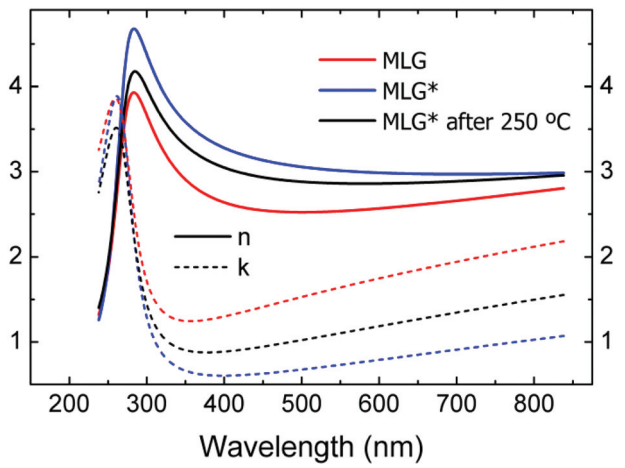

Fig. 12 Refractive index (solid lines) and extinction coefficient (dashed lines) for monolayer graphene obtained for the data measured without thermal treatment fitted using the nominal structure (blue) or the real one (red), and for the data measured after thermal treatment fitted using the nominal structure (black).

of Fig. 5) is compulsory when determining the optical properties of graphene.

Conclusions

The refractive index and extinction coefficient of mass produced graphene samples are determined by ellipsometry analysis. Graphene films were CVD grown on copper substrates and transferred as both monolayers and bilayers onto SiO_2/Si substrates by using standard manufacturing procedures. ARXPS analysis demonstrates the presence of contamination in the form of both an intermediate layer below and an adsorbed layer on top of graphene. Carbon and oxygen are the constituents of the intermediate layer, while oxygen is the main element of the top layer. Therefore the real layered structure used for the ellipsometric analysis has a small amount of carbon included in it with a graphene-like behaviour, probably in the form of small humps, together with water in the intermediate layer, while adsorbed water forms the top layer. This kind of real structure for both, graphene monolayer and bilayer, together with the Lorentz–Drude model proposed, fits successfully the experimental data and allows determination of the effect of the residual debris in the optical response of the whole structure. Therefore, the inclusion of the contaminant layers in the stacked structure is a fundamental step to extract the real graphene refractive index and absorption coefficient. Finally, a simple thermal treatment (150–250 °C for one hour under a nitrogen atmosphere) promotes a dramatic reduction of the water content in the residual layers, proving that it is a feasible method to improve the graphene quality. However, this thermal treatment partially removes the contamination, so the consideration of residue layers is compulsory when determining the optical properties of transferred graphene.

This is the first time that the refractive index and the extinction coefficient are obtained for a standard production of CVD grown graphene with a subsequent transfer taking into account the residual debris impact. Additionally, SE has proven to be a feasible method to determine routinely and in a fast and non-destructive analysis, the graphene and contaminant layers thicknesses. This information can be useful in the development of graphene-based optoelectronic devices for which manufacturers need low-cost methods that could be easily implemented in standard quality control procedures.

Acknowledgements

The authors wish to thank Andrey Chuvilin for TEM images and Gergeley Kronome from SEMILAB for ellipsometry support. S. P. thanks the Spanish MICINN for a Ramón y Cajal fellowship. This work was supported by the Spanish Ministerio de Economía y Competitividad with the projects TEC2011-28639-C02-01 and -02 and with the IPT-2011-1408-420000.

References

1 A. K. Geim and K. S. Novoselov, *Nat. Mater.*, 2007, **6**, 183.
2 G. Kalita, M. S. Kayastha, H. Uchida, K. Wakita and M. Umeno, *RSC Adv.*, 2012, **2**, 3225–3230.

3 N. O. Weiss, H. Zhou, L. Liao, Y. Liu, S. Jiang, Y. Huang and X. Duan, *Adv. Mater.*, 2012, **24**, 5782–5825.
4 J. K. Wassei and R. B. Kaner, *Mater. Today*, 2010, **13**, 52–59.
5 A. Kumar, A. A. Voevodin, D. Zemlyanov, D. N. Zakharov and T. S. Fisher, *Carbon*, 2012, **50**, 1546–1553.
6 Z. Q. Li, E. A. Henriksen, Z. Jiang, Z. Hao, M. C. Martin, P. Kim, H. L. Stormer and D. N. Basov, *Nat. Phys.*, 2008, **4**, 532–535.
7 N. K. Cho, Y. U. Jung, K.-B. Chung and S. J. Kang, *Curr. Nanosci.*, 2013, **9**, 521–524.
8 D.-H. Chae, T. Utikal, S. Weisenburger, H. Giessen, K. v. Klitzing, M. Lippitz and J. Smet, *Nano Lett.*, 2011, **11**, 1379–1382.
9 K. F. Mak, M. Y. Sfeir, Y. Wu, C. H. Lui, J. A. Misewich and T. F. Heinz, *Phys. Rev. Lett.*, 2008, **101**, 196405.
10 Z. Ni, L. Liu, Y. Wang, Z. Zheng, L.-J. Li, T. Yu and Z. Shen, *Phys. Rev. B: Condens. Matter*, 2009, **80**, 125404.
11 R. W. Havener, Y. Liang, L. Brown, L. Yang and J. Park, *Nano Lett.*, 2014, **14**, 3353–3357.
12 Y. Fan, Z. Wei, H. Li, H. Chen and C. M. Soukoulis, *Phys. Rev. B: Condens. Matter*, 2013, **88**, 241403.
13 A. T. Roberts, R. Binder, N. H. Kwong, D. Golla, D. Cormode, B. J. LeRoy, H. O. Everitt and A. Sandhu, *Phys. Rev. Lett.*, 2014, **112**, 187401.
14 V. G. Kravets, A. N. Grigorenko, R. R. Nair, P. Blake, S. Anissimova, K. S. Novoselov and A. K. Geim, *Phys. Rev. B: Condens. Matter*, 2010, **81**, 155413.
15 A. Matković, A. Beltaos, M. Milićević, U. Ralević, B. Vasić, D. Jovanović and R. Gajić, *J. Appl. Phys.*, 2012, **112**, 123523.
16 J. W. Weber, V. E. Calado and M. C. M. van de Sanden, *Appl. Phys. Lett.*, 2010, **97**, 091904–091903.
17 M. Losurdo, M. M. Giangregorio, P. Capezzuto and G. Bruno, *J. Phys. Chem. C*, 2011, **115**, 21804–21812.
18 A. Matkovic, U. Ralevic, M. Chhikara, M. M. Jakovljevic, D. Jovanovic, G. Bratina and R. Gajic, *J. Appl. Phys.*, 2013, **114**, 093505.
19 F. Nelson, A. Sandin, D. B. Dougherty, D. E. Aspnes, J. E. Rowe and A. C. Diebold, *J. Vac. Sci. Technol., B*, 2012, **30**, 04E106-101.
20 A. Matkovic, U. Ralevic, G. Isic, M. M. Jakovljevic, I. Milosevic, D. Markovic and R. Gajic, *Phys. Scr.*, 2012, **T149**, 014069.
21 H. Ju Xu, W. Bing Lu, W. Zhu, Z. Gao Dong and T. Jun Cui, *Appl. Phys. Lett.*, 2012, **100**, 243110.
22 X. Li, W. Cai, J. An, S. Kim, J. Nah, D. Yang, R. Piner, A. Velamakanni, I. Jung, E. Tutuc, S. K. Banerjee, L. Colombo and R. S. Ruoff, *Science*, 2009, **324**, 1312–1314.
23 A. Siokou, F. Ravani, S. Karakalos, O. Frank, M. Kalbac and C. Galiotis, *Appl. Surf. Sci.*, 2011, **257**, 9785–9790.
24 *XPSPeak 4.1*, http://public.wsu.edu/~scudiero/index.html, Accessed 08/19/2014.
25 *SEMILAB*, SEMILAB Semiconductor Physics Laboratory Co. Ltd, 1.3.0 edn, 2014.
26 X. Li, Y. Zhu, W. Cai, M. Borysiak, B. Han, D. Chen, R. D. Piner, L. Colombo and R. S. Ruoff, *Nano Lett.*, 2009, **9**, 4359–4363.
27 M. Baraket, S. G. Walton, Z. Wei, E. H. Lock, J. T. Robinson and P. Sheehan, *Carbon*, 2010, **48**, 3382–3390.
28 F. J. Nelson, V. K. Kamineni, T. Zhang, E. S. Comfort, J. U. Lee and A. C. Diebold, *Appl. Phys. Lett.*, 2010, **97**, 253110–253113.
29 C. Lee, J. Y. Kim, S. Bae, K. S. Kim, B. H. Hong and E. J. Choi, *Appl. Phys. Lett.*, 2011, **98**, 071905.
30 O. Albrektsen, R. L. Eriksen, S. M. Novikov, D. Schall, M. Karl, S. I. Bozhevolnyi and A. C. Simonsen, *J. Appl. Phys.*, 2012, **111**, 064305–064308.
31 P. K. Gogoi, I. Santoso, S. Saha, S. Wang, A. H. C. Neto, K. P. Loh, T. Venkatesan and A. Rusydi, *Europhys. Lett.*, 2012, **99**, 67009.
32 K. F. Mak, J. Shan and T. F. Heinz, *Phys. Rev. Lett.*, 2011, **106**, 046401.
33 L. Yang, *Nano Lett.*, 2011, **11**, 3844–3847.